Study of the Forbush Decreases, Geomagnetic Storms, and Ground-Level Enhancements in Selected Intervals and Their Space Weather Implications

Badruddin[1] · Anand Kumar[1]

Abstract We analysed geomagnetic storms, ground-level enhancements (GLEs), and Forbush decreases in cosmic-ray intensity that occurred in selected intervals. We used data of ground-based neutron monitors for the cosmic-ray intensity. We used the geomagnetic index Dst as a measure of the geomagnetic storm intensity. Solar observations and interplanetary plasma/field parameters were used to identify the solar cause(s), interplanetary structure(s), and physical mechanism(s) responsible for the geomagnetic storms, the Forbush decreases, and the GLEs of different amplitudes and time profiles; all of them occurring within four selected periods of one month each. The observed differences in cosmic-ray and geomagnetic-activity responses to the same solar sources were used to distinguish the structures and mechanisms responsible for transient cosmic-ray modulation and geomagnetic storms.

Keywords Coronal mass ejections · Cosmic rays · Energetic particles · Solar wind · Space weather

1. Introduction

The two most impressive transient changes in cosmic-ray intensity, as observed by ground-based neutron monitors, are ground-level enhancements (GLEs) and Forbush decreases (FDs). On rare occasions, during extreme solar events such as large solar flares and coronal mass ejections (CMEs), particles are accelerated to sufficiently high energies and propagate along the interplanetary magnetic field to Earth. They are detected as a sharp increase in the counting rate of a ground-based cosmic-ray detector and are known as GLEs. Short and sharp increases are recorded over a period of several hours. A number

✉ Badruddin
badr.physamu@gmail.com

1   Department of Physics, Aligarh Muslim University, Aligarh 202 002, India

of GLEs have been detected by ground-based neutron monitors[1] (*e.g.* see Reames, 2009; Papaioannou *et al.*, 2010; Shea and Smart, 2012; Gopalswamy *et al.*, 2012).

Forbush decreases are marked by a sudden decrease in Galactic cosmic-ray (GCR) intensity that reach their maximum depression in about a day, followed by a gradual recovery within a few days. They are generally caused by transient interplanetary events related to CMEs (interplanetary CMEs; ICMEs) from the Sun (*e.g.* Venkatesan and Badruddin, 1990; Cane, 2000; Kumar and Badruddin, 2014). The ICMEs are also the cause of large geomagnetic storms (GSs), characterized by the disturbance storm time index (Dst) as a sharp dip within a few hours, after which the storm gradually recovers its pre-disturbance level within a few days. Although GSs and FDs may have a common solar and interplanetary origin, the magnitudes of GSs and FDs are not proportional to each other (*e.g.* Kudela and Storini, 2005; Kane, 2010), which is perhaps because different mechanisms operate to generate the two phenomena (*e.g.* see Badruddin, Yadav, and Yadav, 1986; Zhang and Burlaga, 1988; Badruddin, Vankatesan, and Zhu, 1991; Sabbah, 2000; Ahluwalia and Fikani, 2007; Alania and Wawrzynczak, 2008; Oh, Yi, and Kim, 2008; Badruddin and Singh, 2009; Subramanian *et al.*, 2009; Yu *et al.*, 2010; Augusto *et al.*, 2012; Dumbovic *et al.*, 2012; Mustajab and Badruddin, 2013; Kane, 2014).

The three phenomena observed at Earth (GLE, FD, and GS) are of considerable significance for space weather research (Kudela and Brenkus, 2004; Reames, 2009; Papaioannou *et al.*, 2010; Mavromichalaki *et al.*, 2011; Shea and Smart, 2012; Gopalswamy *et al.*, 2012; Kudela, 2013). However, two of them, GS and GLEs, are directly responsible for space weather effects, while FD precursors can be useful to predict them. In this work, we analyse the GLEs, FDs, and GSs that occurred within four periods of one month each. The selected months were special in the sense that there was at least one GLE, more than two GS, and also two or more FDs in each month. Two out of four selected months (December 2006 and January 2005) occurred during the low-activity phase (declining phase), the remaining two (April 2001 and July 2000) during the high solar activity (maximum) phase of Solar Cycle 23.

In this study, we analyse neutron monitor data and the geomagnetic Dst index, along with simultaneous near-Earth interplanetary plasma and magnetic-field data during these selected intervals.

2. Geomagnetic Storms: Solar Sources, Interplanetary Structures, and Plasma/Magnetic-Field Conditions

Geomagnetic storms are significant perturbations of the terrestrial magnetic field. The GSs are the results of a final element of a chain of processes that start on the Sun, which disturb the solar wind and the interplanetary medium, and end on Earth. Their origin is related to physical processes in which energy transferred from the solar wind to the terrestrial magnetosphere is redistributed in the coupled magnetosphere-ionosphere system in the form of electric currents. Key questions here are the understanding of these physical processes, and also the ability to predict the occurrence of GSs on the basis of solar and interplanetary observations.

Major GSs are among the most important space weather phenomena because the interaction of solar wind disturbances with Earth's magnetosphere can produce disturbances, and sometimes complete disruptions, of technological systems on Earth and in space around us.

---

[1]http://cosmicrays.oulu.fi/.
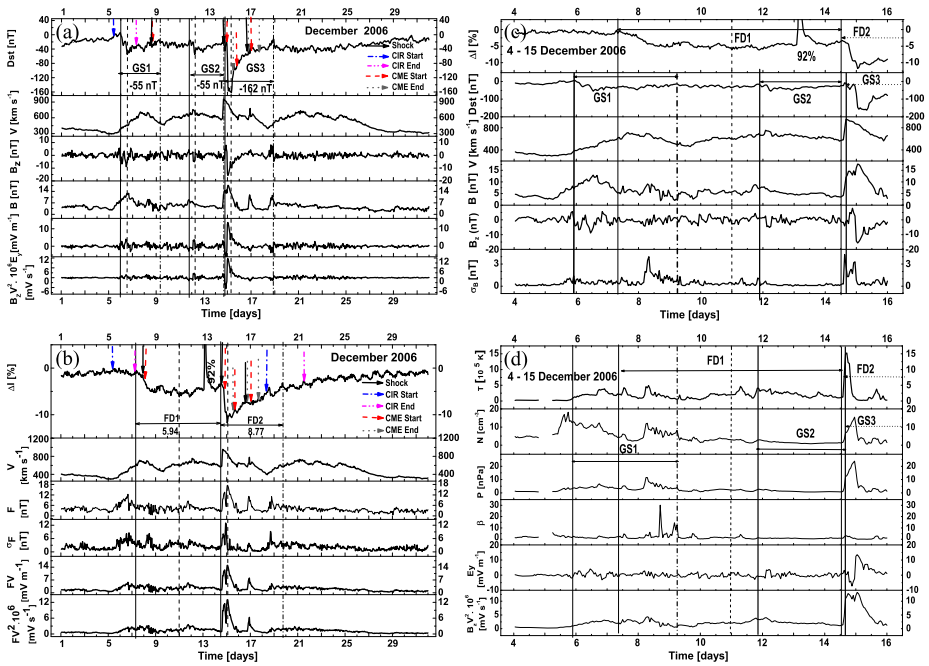
Figure 1 Time variations during December 2006 (hourly data) of (a) the geomagnetic activity index Dst [nT], the solar-wind velocity V [km s^{-1}], the scalar IMF magnitude B [nT], its north–south component B_z [nT], the duskward electric field E_y [mV m^{-1}], and the product $-B_z V^2$ [mV s^{-1}]; the start, minimum, and recovery times of each GS are marked by solid, dashed, and dashed-dotted vertical lines, and (b) the GCR intensity ΔI [%], the solar wind velocity V [km s^{-1}], the vector IMF magnitude F [nT], its standard deviation σ_F [nT] along with the products FV [mV m^{-1}] and FV^2 [mV s^{-1}]; the start, minimum, and recovery times of each FD are marked by solid, dashed, and dashed-dotted vertical lines. In panels (a) and (b) the start and end times of interplanetary structures (shocks/ICMEs/CIRs) are indicated by arrows of different colours. Panels (c) and (d) magnify the portion of 4–15 December 2006, showing ΔI, Dst, V, B, B_z, the field variance of the scalar IMF σ_B [nT], the plasma temperature T [K], the density N [cm^{-3}], the pressure P [nPa], the plasma β-value, E_y, and $B_z V^2$. The start times of FD and GS are shown by thin and thick vertical lines.

A major aim of space weather research is to identify the solar sources, interplanetary drivers of major storms, and their specific features as regards their geo-effectiveness. After these structures are identified, the underlying mechanism that is responsible for generating these storms from different sources has to be explored. It will enable us to distinguish events that are geo-effective from those that are not, and may ultimately enable us to accurately forecast the arrival of geo-effective solar sources.

2.1. December 2006

Figure 1(a) shows the time variations (hourly data) of the geomagnetic index Dst, the solar-wind velocity V, the interplanetary magnetic field (IMF) B (scalar IMF; this is the hourly mean of the IMF magnitude) and its north–south component B_z, the duskward electric field E_y, which has the dimension [mV m^{-1}] of the space-variation of electric potential, and $-B_z V^2$, which has the dimension [mV s^{-1}] of the time-variation of electric potential.
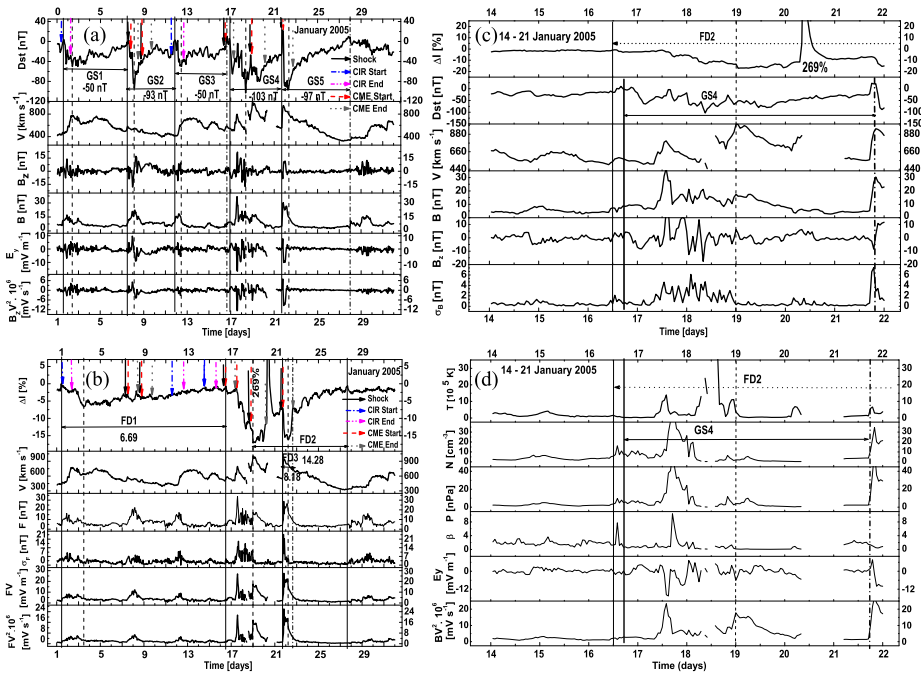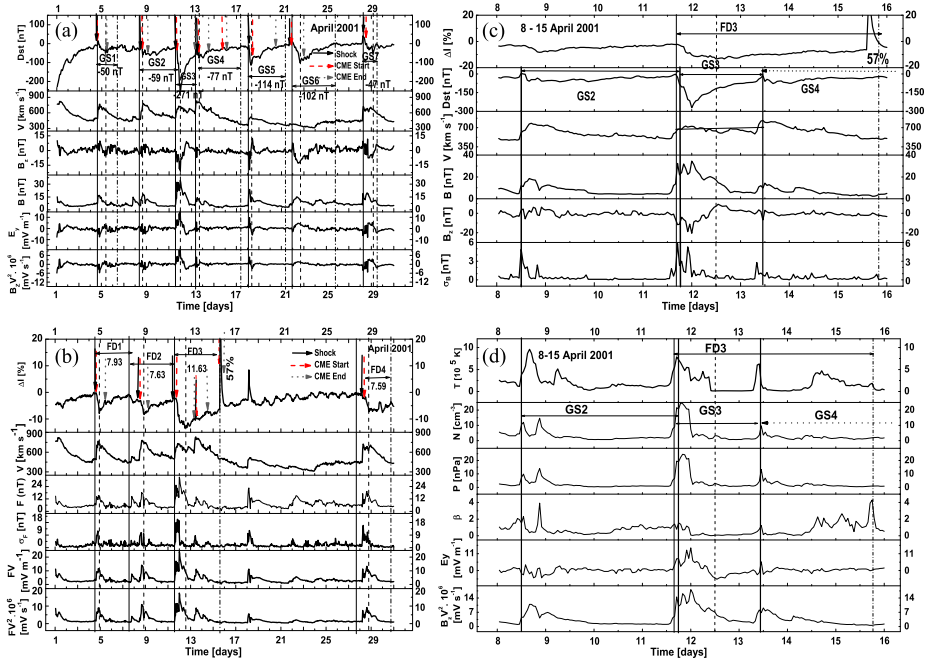
Figure 2 Same as Figure 1, but for the period of January 2005. Panels (c) and (d) show the period of 14 – 21 January 2005 in more detail.

During December 2006, three GSs were identified. They are marked in Figure 1(a) as GS1 (-55 nT), GS2 (-55 nT), and GS3 (-162 nT). GS1 was due to a co-rotating interaction region (CIR), GS2 to a high-speed stream, and GS3, the third and the largest, was due to a magnetic cloud with shock and sheath regions. During the onset of these three storms, the interplanetary parameters B, E_y, and $-B_z V^2$ ($= V E_y$) showed an increase, although of varying magnitude during the different storms. During the onset of GS1, the solar-wind velocity slowly started to increase, it was at its maximum during the onset of GS2, and the increase in velocity was sudden and fast during the onset of GS3. However, B_z became negative during the onset of all three GSs. These GSs, their interplanetary sources, and the plasma- or magnetic field parameters are summarized in Table 1 (electronic supplementary material).

2.2. January 2005

Of the five GSs observed during January 2005, two (GS1 and GS3) were due to CIRs, the remaining three (GS2, GS4, and GS5) were due to CMEs accompanying shocks. They are shown in Figure 2(a). The two GSs due to CIRs were of relatively moderate intensity (Dst $= -50$ nT), while those due to ICMEs produced larger storms (Dst $= -93$ nT, -103 nT, and -97 nT). Not only the sizes were different, but the time profiles of these storms differed as well; GS1 was a slowly varying storm, GS2 was a two-step storm, GS3 was a typical storm of moderate intensity, GS4 was a multi-step storm due to a number of ICMEs, and GS5 was a single-step storm showing a sudden commencement at the time of onset. Differences in time variations in various parameters during different storms are
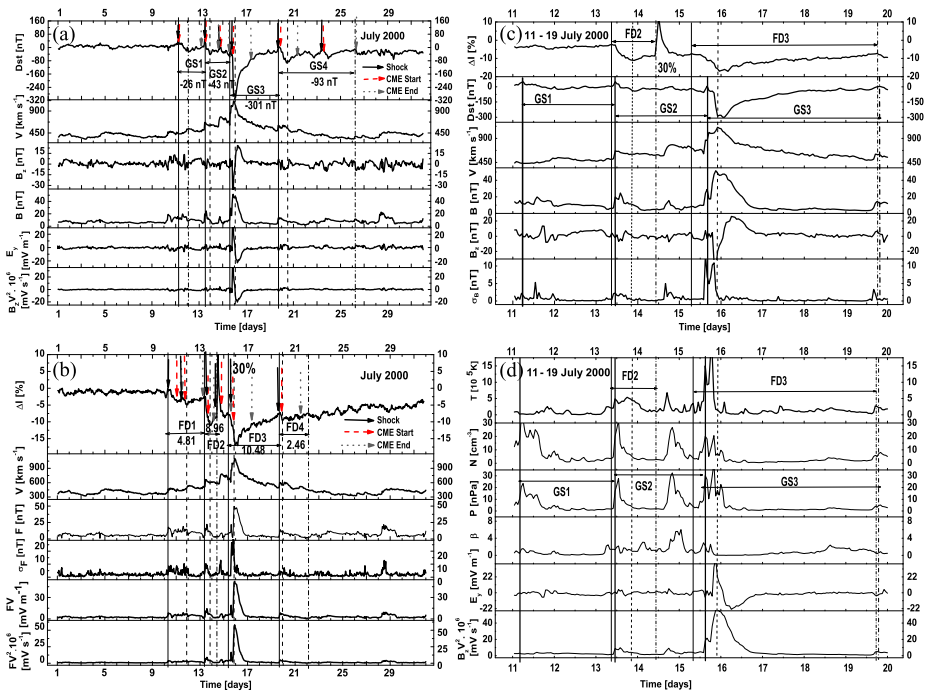
Figure 3 Same as Figure 1, but for the period of April 2001. Panels (c) and (d) show the period of 8–16 April 2001 in more detail.

evident in Figure 2(a). The sources and amplitudes of various parameters are summarized in Table 2 (electronic supplementary material). The properties of interplanetary parameters worth mentioning are as follows: B_z was fluctuating during the main phase of GS1 associated with the CIR, the solar wind velocity was comparatively low, but B_z was highly negative (-18.2 nT) during the onset of GS2, B_z and E_y were highly fluctuating during the multiple-step GS4, and B_z was negative for a very short time at the onset of GS5, but both V and B increased abruptly to a high value almost at the same time.

2.3. April 2001

We selected a period (April 2001) of high solar activity in Cycle 23. During this month, seven geomagnetic storms were observed (Figure 3(a)). All of these GSs were due to ICMEs that accompanied shocks (Table 3, electronic supplementary material). The largest one (Dst $= -271$ nT), *i.e.* GS3, was a two-step storm associated with the passage of a shock or sheath region followed by a magnetic cloud. Although the solar wind velocity was moderately high, the IMF B_z (-20.5 nT) was quite large and southward. The duskward electric field was also the strongest (-14.6 mV m^{-1}) of all the seven events. The complete recovery of this storm was prolonged by the occurrence of other ICMEs in the recovery phase. Another storm (GS6, Dst $= -102$ nT) is worth mentioning; this event occurred during the passage of a very low speed structure (speed < 400 km s^{-1}), but the IMF B_z was reasonably large (-12.8 nT) and oriented southward for a relatively long time.

Figure 4 Same as Figure 1, but for the period of July 2000. Panels (c) and (d) show the period of 11 – 20 July 2000 in more detail.

2.4. July 2000

During July 2000, four GSs (GS1, GS2, GS3, and GS4) were observed in succession (Figure 4(a)) between 11 July and 25 July due to a disturbed solar wind condition that was a result of several ICMEs reaching Earth (Table 4, electronic supplementary material). The largest of these four, GS3 (Dst $= -301$ nT), was due to a magnetic cloud that accompanied a shock. Although two smaller storms preceded this event (Figure 4(a)), its main phase was very sharp. It was due to a very fast interplanetary structure ($V > 1000$ km s^{-1}); both the IMF B_z (-45.3 nT) and E_y (47.11 mV m^{-1}) were very large. Other parameters $B = 51.6$ nT and $B_z V^2 = 50$ mV s^{-1} were also unusually large. All the four GSs, their responsible structures, and their plasma and field parameters are summarized in Table 4.

2.5. Summary

A summary of all the GSs of four selected months (December 2006, January 2005, April 2001, and July 2000), discussed above, is given in Table 5 (electronic supplementary material).

We performed a linear regression analysis of all the GS events between the amplitudes of Dst (Dst$_{min}$) and the amplitudes of the plasma or magnetic field parameters during the passage of corresponding interplanetary structures, i.e., V_{max}, $(B_z)_{min}$, B_{max}, $(E_y)_{max}$, and $(E_y V)_{max}$ (Figure 5). We found the correlations, in order of increasing correlation coefficients R, between Dst$_{min}$ and other parameters to be Dst$_{min}$ and V_{max} ($R = -0.45$), B_{max} ($R = -0.74$), $(-B_z V^2)_{max}$ ($R = -0.80$), $(E_y)_{max}$ ($R = -0.85$), and $(B_z)_{min}$ ($R = 0.88$).
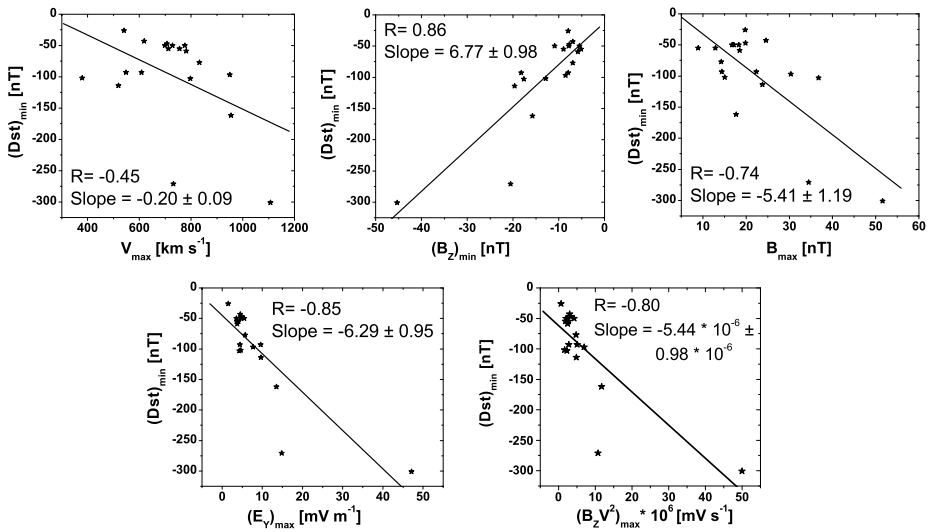
Figure 5 Scatter plots and correlation coefficients (R) between Dst_{min} and the amplitudes of various interplanetary plasma or magnetic field parameters due to GS observed in the selected periods.

The ratio of the change in Dst against the change in B_z or E_y was also calculated from the linear fit; it is found to be $\Delta Dst/\Delta B_z = 6.77 \pm 0.98$ and $\Delta Dst/\Delta E_y = -6.29 \pm 0.96$.

3. Forbush Decreases: Solar Sources, Interplanetary Structures, and Plasma/Field Conditions

Forbush decreases are characterized by rapid reduction (within a few hours) in cosmic-ray intensity followed by a slow recovery that typically lasts several days. A typical FD at Earth is caused by an ICME or by a CIR; they suppress the intensity of GCRs coming through interplanetary space. On Earth, neutron monitors and muon detectors continuously record the GCR intensity; these detectors also detect the FDs on Earth and provide information about their onset, amplitude, and time profile.

Before the FD onset, one may forecast space weather by referring to precursor anisotropies. The 'loss-cone' precursor anisotropy before the FD predicts the arrival of an interplanetary shock and the associated ICME. Precursor decreases in GCR intensity may occur from a 'loss-cone' effect due to particles whose trajectories are traced back to the region of depleted cosmic-ray particles behind the shock, while precursor increases may result from the particles that have received a small energy boost by reflection from the approaching shock. Thus the study of solar sources and interplanetary structures responsible for FDs is also important from the point of view of space weather prediction.

3.1. December 2006

In December 2006, two large FDs were recorded by neutron monitors. In one of them (FD1) the GCR intensity decreased to 5.94 %, in the other (FD2) it decreased to 8.77 % as observed at the Oulu neutron monitoring station. In the first case, the decrease to minimum intensity (main phase) was slow, while in the case of second FD, the decrease was very fast. The GCR

intensity in FD1 remained depressed for several days, while in FD2 the intensity started to recover after a few hours. The recovery in the latter case was long, probably because several ICMEs arrived during the recovery phase. During the recovery phase of FD1, a GLE of 92 % occurred.

To understand the mechanism that is mainly responsible for these decreases of different type, amplitude, and time profile, we plot in Figure 1(b) simultaneous data of the solar wind velocity V, the vector IMF magnitude F (*i.e.* the absolute value of hourly mean IMF vector), the standard deviation in vector IMF magnitude σ_F, and two quantities FV and FV^2. The product FV has the dimension of the electric field [mV m^{-1}], FV^2 has the dimension of the time variation of the electric potential [mV s^{-1}]. FD1 was associated with a high-speed stream and an ICME. The intensity depression was slow but remained depressed for quite a long time (a few days). Although the velocity V remained enhanced for a longer period, the IMF magnitude F was not very high, but it fluctuated during this period. The other parameters FV and FV^2 were enhanced compared with the initial conditions. In FD2 a classical FD was initiated by a shock associated with a magnetic cloud. Here the parameters V, F, σ_F, FV, and FV^2 were enhance to quite high values (Table 1) during the declining phase. The main phase lasted while σ_F was high, and the recovery started when σ_F reached almost its initial level. Although the interplanetary parameters (V, F, FV, and FV^2) remained enhanced, their values reached the initial level about a day after the recovery started. In other words, the recovery in GCR intensity started about a day before the interplanetary parameters resumed normal level. This probably indicates the importance of the magnetic field turbulence, indicated by enhanced σ_F, in depressing the GCR intensity.

The comparison of Figures 1(a) and 1(b) is interesting because it provides similarities and differences in the geo-effectiveness and GCR-effectiveness of ICMEs, high-speed streams, and CIRs, and shows the relative importance of various parameters during GS and FD events that occurred in December 2006.

3.2. January 2005

In January 2005, the first Forbush decrease (FD1) of 6.69 % due to a CIR was identified in ACE data[2] on 1 January 2005. FD1 was a decrease that reached its lowest level of intensity in two steps and then slowly recovered its initial level in about two weeks. During the recovery, two ICMEs, one on 7 January and other on 8 January, and a CIR on 11 January probably prolonged the recovery (see also Papaioannou *et al.*, 2010). The second Forbush decrease (FD2) was a multi-step cosmic-ray decrease of 14.28 % that started on 16 January, 11:00 UT, and reached the minimum level in three sharp steps. However, as it started recovering, within two days a GLE caused by a strong solar flare (location N12W58) occurred (Reames, 2009). Within a day of GLE occurrence, an ICME accompanying a shock produced a transient decrease (FD3) with a duration of one day. To search for the interplanetary causes of the intensity decreases of different nature, amplitudes, and time profiles, we show in Figure 2(b) the time profiles of V, F, σ_F, FV, and FV^2. For the CIR-associated FD (FD1), the vector IMF magnitude F and related parameters (σ_F, FV, and FV^2) were not much enhanced. However, for the cosmic-ray 'storm' (FD2), the field enhancement was quite strong and fluctuated; enhancements in σ_F persisted for extended periods of about two days in three steps, almost corresponding to the times of the step-wise intensity decreases. It is interesting to note that after the extended region of the turbulent magnetic field passed (enhanced σ_F), the intensity started recovering even though the

---

[2]http://www-ssc.igpp.ucla.edu/~jlan/ACE/Level3/.

magnetic field was enhanced for a few more hours. The GLE occurred during the period of weak (low F) and quiet (low σ_F) magnetic field. FD3, a transient decrease of 8.18 % of U-shape (recovering very fast) occurred as a result of an ICME that accompanied a shock. In this case, there was only a sharp spike in σ_F at the shock arrival. Such a quick recovery is rare for a decrease of this amplitude (8.18 %). The ICMEs and CIRs observed during this period, FD amplitudes, and the peak values of various parameters (F_{max}, V_{max}, $(\sigma_F)_{max}$, $(FV)_{max}$, and $(FV^2)_{max}$) are summarized in Table 2. A comparison of Figures 2(a) and 2(b) and Table 2 shows the difference in 'geo-effectiveness' and 'GCR effectiveness' of individual interplanetary structures; the former being mainly due to reconnection between interplanetary and Earth's magnetic fields (*e.g.* see Badruddin and Singh, 2009; Mustajab and Badruddin, 2013), the latter mainly to scattering of cosmic-ray particles by magnetically turbulent field regions (see *e.g.* Badruddin, Yadav, and Yadav, 1986; Zhang and Burlaga, 1988; Badruddin, Vankatesan, and Zhu, 1991; Badruddin, 2002; Oh, Yi, and Kim, 2008; Yu *et al.*, 2010; Kumar and Badruddin, 2014).

3.3. April 2001

In April 2001, four FDs were detected with amplitudes > 7 %. The largest had an amplitude of 11.63 %. All these FDs were caused by ICMEs that accompanied shocks (Figure 3(b) and Table 3). In all these cases, FDs started at the arrival of the shock and reached the minimum level within few hours (< 24 h). During their main phase, the interplanetary parameters V, F, σ_F, FV, and FV^2 increased; the major decrease took place when σ_F was enhanced, however, indicating the passage of turbulent field region. Both F and σ_F were very high ($F = 25.4$ nT, $\sigma_F = 20.3$ nT) during the passage of the structure responsible for the largest FD, *i.e.* FD3. The recovery of FD3 was very slow. Another interesting aspect of FD3 was that a large GLE of 57 % was recorded during its recovery phase.

3.4. July 2000

In July 2000, four FDs of different amplitudes could be identified. The interplanetary origin of these FDs could be traced to ICMEs with shocks passing Earth. The amplitude of these FDs, in order of increasing amplitudes, were 2.46 % (FD4), 4.81 % (FD1), 8.96 % (FD2), and 10.48 % (FD3); see Figure 4(b) and Table 4. At least for the large FDs (FD1, FD2, and FD3), the decrease started at the arrival of the shock, and the main phase of decrease was observed until σ_F reached the normal level, although other parameters (V, F, FV, and FV^2) remained enhanced for some more time. A GLE of 30 % amplitude was observed during the recovery of FD2.

3.5. Summary

The FDs observed during the four selected months, the structures that caused them, and the peak values of the plasma or magnetic field parameters are summarized in Table 5 (electronic supplementary material). A correlation analysis of FD amplitudes and amplitudes of the plasma or magnetic-field parameters shows that an 'enhanced and turbulent magnetic field' was the most appropriate interplanetary condition for FDs to occur, and their enhancement appeared to determine the amplitude of FDs. From the data plotted in Figure 6, it is found that on the average, GCR intensity during the FDs decreased at a rate of about 0.2 % per nT change in magnetic field during the passage of an enhanced and turbulent field region.
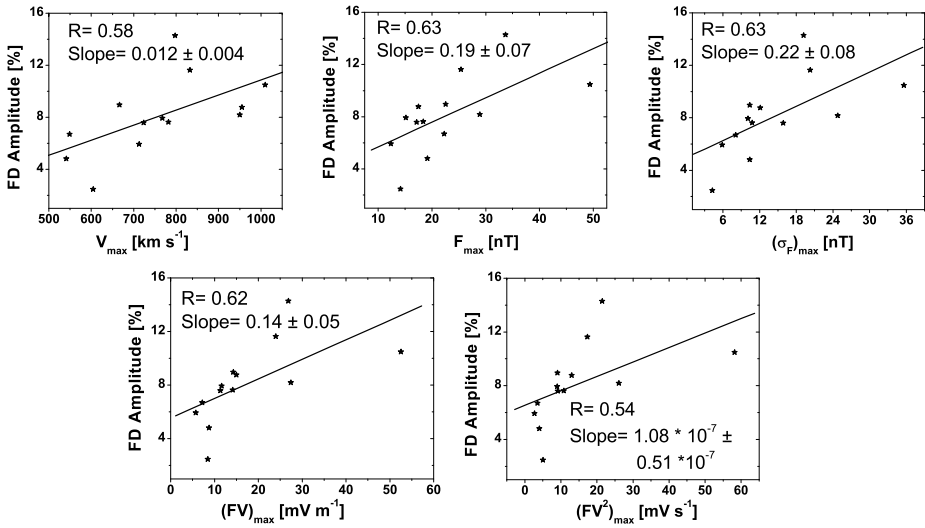
Figure 6 Scatter plots and correlation coefficients (R) between FD amplitude [%] and the amplitudes of various interplanetary plasma or magnetic field parameters observed in the selected periods.

Figures 1(b) – 4(b) show the GCR intensities during the studied periods recorded at the neutron monitor located at Oulu in Finland (latitude: 65.02° N, longitude: 25.5° E, cut-off rigidity: 0.81 GV, median energy: 10.30 GeV). However, the intensity and the amplitude of a FD recorded at different locations on Earth are different. The detectors located at different latitudes respond to different median energies of the particles, related to cut-off rigidities (see Usoskin *et al.*, 2008). We selected eight events for which data were available for a number of neutron monitors with a range of median energy E_m, and studied the FD amplitude as a function of E_m. The FD amplitude decreases roughly as $E_m^{-\gamma}$, and the energy exponent γ was found to vary from ≈ 0.5 to ≈ 1. A detailed study is needed to understand these variations in the energy exponent and its relation, if any, to the type of responsible structures and their associated features.

We also examined the dependence of the energy exponent γ, if any, on the amplitudes of FDs and solar plasma and field parameters such as V_{max}, F_{max}, $(\sigma_F)_{max}$, and $(FV)_{max}$. We found very weak, decreasing trends in γ against these parameters, but again, a physical reason needs to be assigned to these dependences.

4. Ground-Level Enhancements: Solar Sources, Interplanetary Structures, and Plasma/Field Conditions

Ground-level enhancements are a subset of solar energetic particle (SEP) events that are observed by ground-based neutron monitors as sudden enhancements in cosmic-ray flux when the energy of accelerated particles in solar flares or in the interplanetary space exceeds the atmospheric threshold and geomagnetic cut-off (Gopalswamy *et al.*, 2012). The acceleration of particles to high energies ($\approx$ GeV) on timescales of seconds to minutes as well as their propagation through space is still not well understood. Currently, there are no known methods to predict from initial solar observations whether a specific solar activity will produce a GLE because we have yet to identify unique signatures for the initiation of a flare/CME that
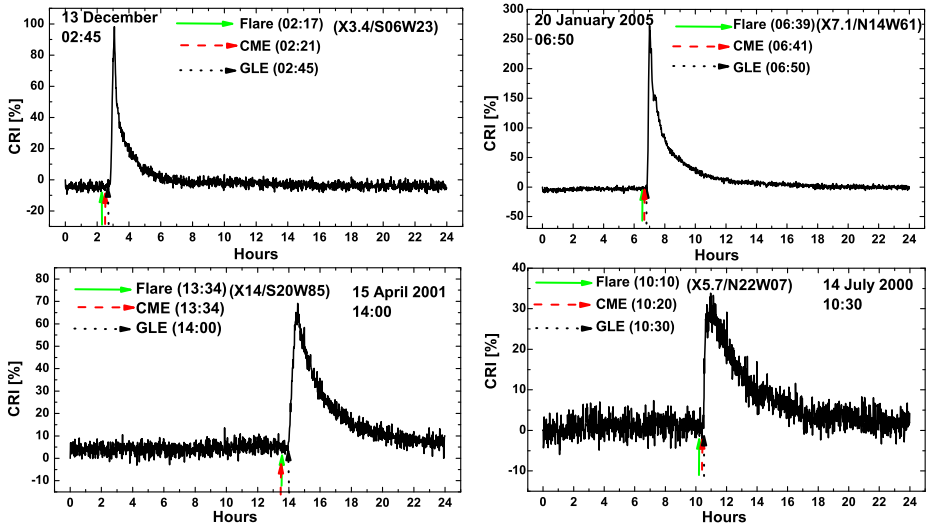
Figure 7 Four different GLEs as observed by the Oulu neutron monitor. The timings of flare, CME, and GLE start are also shown.

would indicate an imminent explosion and its probable onset time, location, and strength. Furthermore, the size of GLEs is highly variable. Understanding the solar and interplanetary conditions in which GLEs are generated is vital, and efforts made to understand them should continue. It is important to search for the primary characteristics of a flare or CME that is responsible for GLEs. It is also important to identify the condition at which acceleration is most efficient.

Four large GLEs were observed, one in each of four selected periods. The Oulu neutron monitor plots (one-minute data) of the GLEs are shown in Figure 7. The time and location of the flares on the Sun that have been suggested to be responsible for these GLEs are also given. The timing of CMEs after the flare is also indicated. The amplitudes are different in the data from other neutron monitor stations with different cut-off rigidities. All the four GLEs of different amplitudes were associated with X-class western flares, which should be well connected to Earth via the interplanetary magnetic field.

As mentioned earlier, we selected periods when three prominent phenomena, namely, FD, GS, and GLE were observed within certain periods, if not simultaneous. A comparison between panels (a) and (b) of Figures 1 – 4 shows that an ICME/CIR that was strongly geo-effective was not necessarily strongly GCR-effective. Similarly, an ICME/CIR that produced a large FD was not necessarily strongly geo-effective. Moreover, we observed from Figures 1(b) – 4(b) that all the four GLEs occurred during the recovery phase of FDs. To examine this difference in more detail, in the GCR-effectiveness and Geo-effectiveness of some of the interplanetary structures, and the near-Earth plasma and field conditions in which these four GLEs were detected at Earth, we produced the 'expanded' figures with simultaneous plots of cosmic-ray intensity ΔI, geomagnetic index Dst, and interplanetary plasma/magnetic-field parameters: V, B, B_z, standard deviation in scalar IMF (σ_B), solar-wind plasma temperature T, density N, pressure P, plasma β-value, Ey, and $B_z V^2$. The parameters σ_B, T, N, and β help to identify or distinguish the regions of interplanetary structure such as shock, sheath, or CME, as changes in these parameters are distinct during their passage.

Figures 1(c) and 1(d) are such expanded figures that contain the GLE of December 2006. There we observe that (a) the GLE of 13 December 2006 occurred during the recovery phase of a FD, (b) the GLE was observed when the near-Earth interplanetary condition was magnetically 'quiet', and (c) the onset times of FDs and GS due to the same interplanetary structure were not simultaneous. Figures 2(c) and 2(d) show a period in January 2005 containing the GLE of 20 January 2005. These figures show that (a) the GLE occurred during the recovery phase of a FD, (b) GLE was observed when B and σ_B were very low (magnetically quiet condition), and (c) a GS started on 16 January, but there was no FD onset at that time. Figures 3(c) and 3(d) show a period containing the GLE that was observed in April 2001. Again, we observe that the GLE occurred during the recovery phase of a FD when the solar-wind velocity was low and the interplanetary field condition was quiet. The GLE that was observed in July 2000 (Figures 4(c) and 4(d)) also occurred during the recovery phase of a FD. This GLE was observed during low B and low σ_B condition (*i.e.* quiet magnetic field), and the FD started earlier than the GS due to the same interplanetary structure.

5. Conclusions

From this study we conclude the following:

1) An ICME or CIR may not be necessarily geo-effective as well as GCR-effective, probably because different mechanisms generate GS and FDs.
2) A CME that develops as a sheath or magnetic cloud structure in the interplanetary space appears to be more 'geo-effective' as well as 'GCR-effective'; however, the one-to-one correspondence is not obvious.
3) In accord with earlier findings, the most effective interplanetary parameter for geo-effectiveness of ICME appears to be the southward magnetic field and the duskward electric field, while for the geo-effectiveness of CIR the north–south fluctuating magnetic field appears more important for it to be geo-effective.
4) The important interplanetary parameter for 'GCR-effectiveness' appears to be the enhanced and turbulent magnetic field. Scattering of cosmic-ray particles by an enhanced turbulent magnetic field in the sheath region between the shock front and the CME or magnetic cloud appears to be the most effective mechanism to produce FDs in cosmic rays. Following the passage of the shock or sheath structure, the GCR intensity started to slowly recover.
5) The energy exponent of FDs does not appear to depend on the level of enhancements in the interplanetary plasma or field parameters and/or the type of responsible interplanetary structures; the speed of the responsible interplanetary structure appears to have some relationship with the energy exponent of FDs, however.
6) All of the four GLEs studied in this work occurred during the recovery phase of FDs. These GLEs were observed when the near-Earth interplanetary field condition was magnetically quiet at 1 AU.

References

Ahluwalia, H.S., Fikani, M.M.: 2007, *J. Geophys. Res.* **112**, A08105.
Alania, M.V., Wawrzynczak, A.: 2008, *Astrophys. Space Sci. Trans.* **4**, 59.

Augusto, C.R.A., Kopenkin, V., Navia, C.E., Tsui, K.H., Shigueoka, H., Fauth, A.C., *et al.*: 2012, *Astrophys. J.* **759**, 143.

Badruddin: 2002, *Astrophys. Space Sci.* **281**, 651.

Badruddin, Singh, Y.P.: 2009, *Planet. Space Sci.* **57**, 318.

Badruddin, Vankatesan, D., Zhu, B.Y.: 1991, *Solar Phys.* **13**, 203.

Badruddin, Yadav, R.S., Yadav, N.R.: 1986, *Solar Phys.* **105**, 413.

Cane, H.V.: 2000, *Space Sci. Rev.* **93**, 55.

Dumbovic, M., Vrsnak, B., Calogovic, J., Zupar, R.: 2012, *Astron. Astrophys.* **548**, A28.

Gopalswamy, N., Xie, H., Yashiro, S., Akiyama, S., Mäkelä, P., Usoskin, I.G.: 2012, *Space Sci. Rev.* **171**, 23.

Kane, R.P.: 2010, *Ann. Geophys.* **28**, 479.

Kane, R.P.: 2014, *Solar Phys.* **289**, 2669.

Kudela, K.: 2013, *J. Phys. Conf. Ser.* **409**, 012017.

Kudela, K., Brenkus, R.: 2004, *J. Atmos. Solar-Terr. Phys.* **66**, 1121.

Kudela, K., Storini, M.: 2005, *J. Atmos. Solar-Terr. Phys.* **67**, 907.

Kumar, A., Badruddin: 2014, *Solar Phys.* **289**, 2177.

Mavromichalaki, H., Papaioannou, A., Plainaki, C., Sarlanis, C., Souvatzoglou, G., Gerontidou, M., *et al.*: 2011, *Adv. Space Res.* **47**, 2210.

Mustajab, F., Badruddin: 2013, *Planet. Space Sci.* **82–83**, 43.

Oh, S.Y., Yi, Y., Kim, Y.H.: 2008, *J. Geophys. Res.* **113**, A01103.

Papaioannou, A., Malandraki, O., Belov, A., Skoug, R., Mavromichalaki, H., Eroshenko, E., Abunin, A., Lepri, S.: 2010, *Solar Phys.* **266**, 181.

Reames, D.V.: 2009, *Astrophys. J.* **706**, 844.

Sabbah, I.: 2000, *Geophys. Res. Lett.* **27**, 1823.

Shea, M.A., Smart, D.F.: 2012, *Space Sci. Rev.* **171**, 161.

Subramanian, P., Antia, H.M., Dugad, S.R., Goswami, U.D., Gupta, S.K., Hayashi, Y., *et al.*: 2009, *Astron. Astrophys.* **494**, 1107.

Usoskin, I.G., Braun, I., Gladysheva, O.G., Hörandel, J.R., Jämsén, T., Kovaltsov, G.A., Starodubtsev, S.A.: 2008, *J. Geophys. Res.* **113**, A07102.

Venkatesan, D., Badruddin: 1990, *Space Sci. Rev.* **52**, 121.

Yu, X.X., Lu, H., Le, G.M., Shi, F.: 2010, *Solar Phys.* **263**, 227.

Zhang, G., Burlaga, L.F.: 1988, *J. Geophys. Res.* **93**, 2511.